Detailed Investigation of Phenol Degradation on Au/TiO_2 Composite Materials

Article *in* Journal of Nanoscience and Nanotechnology · January 2019

DOI: 10.1166/jnn.2019.15793

CITATIONS
5

READS
252

6 authors, including:

Zsejke Réka Tóth
Babeş-Bolyai University
18 PUBLICATIONS **71** CITATIONS
SEE PROFILE

Zsolt Pap
Babeş-Bolyai University
105 PUBLICATIONS **1,094** CITATIONS
SEE PROFILE

Virginia Danciu
Babeş-Bolyai University
140 PUBLICATIONS **1,311** CITATIONS
SEE PROFILE

Veronica Cosoveanu
Babeş-Bolyai University
57 PUBLICATIONS **471** CITATIONS
SEE PROFILE

Article

Journal of
Nanoscience and Nanotechnology
Vol. 19, 407–413, 2019
www.aspbs.com/jnn

Detailed Investigation of Phenol Degradation on Au/TiO_2 Composite Materials

Zsejke-Réka Tóth[1, 2, †], Zsolt Pap[2, 3, †], Virginia Danciu[4], Veronica Cosoveanu[4], Lucian Baia[2, 5], and Gábor Kovács[1, 2, 3, *]

[1] Department of Applied and Environmental Chemistry, University of Szeged, Rerrich Béla tér 1, HU-6720, Szeged, Hungary
[2] Nanostructured Materials and Bio-Nano-Interfaces Center, Institute for Interdisciplinary Research on Bio-Nano-Sciences, Babeş-Bolyai University, 400271 Cluj-Napoca, Romania
[3] Institute of Environmental Science and Technology, Tisza Lajos krt. 103, HU-6720, Szeged, Hungary
[4] Faculty of Chemistry and Chemical Engineering, Babeş-Bolyai University, Arany János 11, RO-400028 Cluj-Napoca, Romania
[5] Faculty of Physics, Babeş-Bolyai University, M. Kogălniceanu 1, RO–400084 Cluj–Napoca, Romania

Photocatalytic applicability of different TiO_2-based nanomaterials is a current hot topic. Therefore, our interest for the present research was to elucidate the formation of primary and secondary intermediates during the phenol degradation by photocatalysis, in the presence of Au/TiO_2 nanocomposites. The composites consisted of differently shaped gold nanoparticles and commercial titania (Evonik Aeroxide P25). The obtained composites and the noble metal nanoparticles' morphology was investigated by Transmission Electron Microscopy (TEM), their optical properties were explored using Diffuse Reflectance Spectroscopy (DRS), while the crystal structure was characterized by X-ray diffraction (XRD). The photocatalytic activity was investigated by photodegradation of phenol and methyl orange. In case of phenol it was shown that, the formation of degradation intermediates, was dependent on the Au nanoparticles' shape, leading to high amounts of different intermediates as follows: hydroquinone for composites with spherical Au nanoparticles, 1,2,4-trihydroxy-benzene for triangle shaped nanoparticles, and pyrocatechol for TiO_2.

Keywords: Photocatalysis, UV Light, (Model) Organic Pollutants, Shape-Tailoring, Gold Nanoparticles.

1. INTRODUCTION

One of the most important class of organic contaminants is phenol and its derivatives. Phenol is classified as a hazardous pollutant with an $LD_{50} = 317\ mg \cdot kg^{-1}$ (in the case of mice, oral administration) and multiple applicability (e.g., pesticides and pharmaceutical industry). Methyl orange is also a hazardous pollutant with an LD_{50} value of $60\ mg \cdot kg^{-1}$ (in the case of mice, oral administration). In order to remove these compounds, heterogeneous photocatalysis is a feasible approach.

TiO_2 is one of the most intensively investigated photocatalyst, with benefic properties such as chemical inertness, strong oxidizing power, non-toxicity, relatively cheap production costs and environmentally friendliness.[1] TiO_2 is active only in UV light, therefore composites with different semiconductors were conceived, such as with WO_3 to extend the action spectrum[2] or ZnO to enhance the UV activity[3] of the chosen titania. Another approach to extend the photocatalytic activity of TiO_2 in visible light was the combination with noble metals (such as Au,[4] Ag,[5] Pt,[6] Pd[7]) or even carbon-based materials (nanowires, nanotubes[8]). Gold nanoparticles possess a handful of favorable properties, including non-toxicity, stability and biocompatibility. The application of gold nanoparticles increased continuously in the last two decades: as catalysts, sensors,[9] cancer diagnostics and therapy agents,[10, 11] conjugation of gold nanoparticles in antibodies.[12]

A large spectrum of gold nanoparticles were obtained and used for photocatalytic purposes (e.g., wires,[13] cubes,[14] spheres,[13] triangles,[15] gold nanocages using indirect[16] and direct[17] synthesis pathways) investigating different reaction parameters and pathways (e.g., electrochemical reaction[18]/photochemical methods[19]). Au/TiO_2

*Author to whom correspondence should be addressed.
†These two authors contributed equally to this work.

nanocomposites were also used for the degradation of several model pollutants such as: methyl orange and methylene blue,[20,21] phenol,[22] 4-chlorophenol[23] (both under UV and visible light). To degrade the mentioned model pollutants, the generation of $^{\cdot}OH$ radicals is mandatory, which can be done by the conversion of $O_2^{-\cdot}$ into hydrogen peroxide which finally can be transformed into $^{\cdot}OH$ radicals.[24]

The chosen catalytic or photocatalytic process should follow several requirements such as the possible formation of degradation intermediates and their physico-chemical properties and eco-safety. The latter one means that if the degradation of phenol is targeted, then the resulting products must be less toxic than phenol itself. Grabowska et al. showed 28 different intermediates in the case of phenol degradation,[25] which have different LD_{50} values. Phenol has a 317 $mg\cdot kg^{-1}$ LD_{50} value, while their primary intermediates such as Pyrocatechol (PY, Hydroquinone (HQ) and Resorcinol (Res) (LD_{50}: HQ – 320 $mg\cdot kg^{-1}$, Res – 310 $mg\cdot kg^{-1}$, Py – 260 $mg\cdot kg^{-1}$) show different toxicity levels. During the phenol degradation, in the first step, the ortho and the para hydroxylated intermediates are favored. The as formed intermediates adsorb at the catalysts surface, therefore they can slightly inhibit the phenol degradation process.[26]

Considering the above-mentioned aspects, it was important to investigate the effect of differently shaped Au nanoparticles deposited on the surface of titania on the degradation intermediates formed during the photodegradation of phenol and on the degradation efficiency of methyl orange in order to evaluate, how enlargeable can be the applicability spectra of the as prepared composites and how the efficacies obtained for phenol are correlating with methyl orange.

2. EXPERIMENTAL SECTION

2.1. Materials

The TiO_2/Au composites were prepared by using $HAuCl_4\cdot 3H_2O$ (Sigma-Aldrich), as the precursor, trisodium citrate (Alfa Aesar), oleylamine, and CTAB (both from Sigma-Aldrich) as shape control agents.

Evonik Aeroxide P25 (*abbreviated as* TiO_2) was obtained from Evonik Industries, and it was used as received. All chemicals were of analytical grade.

2.2. Nanoparticle's Synthesis

2.2.1. Nanoparticle's Synthesis by Chemical Reduction

2.2.1.1. Synthesis of the Au Nanoparticles with Different Morphologies. Based on our previous work,[27] the gold *nanowires* were obtained using 25 mL of oleylamine, heated and kept at 75 °C and 0.100 g of $HAuCl_4\cdot 3H_2O$ dissolved in 1 mL ethanol. The solution was added to oleylamine and kept for 6 hours under inert (N_2) atmosphere (*without stirring*). After 6 hours, the reaction products were cooled down to room temperature and centrifuged with 3 × 25 mL ethanol (1 × 16 min 4400 rpm, 2 × 8 min 4400 rpm) and 1 × 25 mL methanol (8 min, 4400 rpm). The *nanospheres* were synthetized similarly as described above, the only difference was in the reaction temperature, which was set to 85 °C.

2.2.1.2. The Synthesis of the Composites. In all composites the mass ratio between the components were 99:1 = TiO_2:Au.

The as obtained *nanowires* were dispersed in 100 mL hexane. In the next step, 800 mg of TiO_2 was dispersed in 50 mL hexane, and afterwards 6.46 mL of nanowires-hexane mixture was added to this suspension. Finally, it was dried for 24 hours at 40 °C. (*Abbreviation: TiO_2/Au_W*).

The 4 mL from the obtained *nanospheres* was added into TiO_2 (suspension concentration was 5.3 $g\cdot L^{-1}$, introducing 800 mg TiO_2 in 150 mL MQ H_2O) suspension. In the next step, it was dried for 24 h, at 40 °C. After this, it was cleaned using centrifugal washing, with acetone (3 × 50 mL, 4400 rpm, 10 min). Finally, it was dried once more for 24 h, at 40 °C. (*Abbreviation: TiO_2/Au_S*).

Au-nanotriangles based composites were obtained using the product from Section 2.2.1.1. 83.63 mL from the as obtained sol was added into 800 mg TiO_2/150 mL H_2O suspension. The product was dried for 24 h at 40 °C and after drying, it was centrifuged with 3 × 25 mL H_2O and dried once more (24 hours, 40 °C). (*Abbreviation: TiO_2/Au_T*).

2.2.2. Nanoparticle's Synthesis by Photoreduction Method

The composites synthetized using the photoreduction method was described in a previous work of our group.[28] Briefly, 800 mg of TiO_2 was added to oxalic acid solution (50 mM) (4 $g\cdot L^{-1}$) and afterwards 3.22 mL of gold precursor solution (12.7 mM) was added to the mixture. The as obtained suspension was stirred for 5 h under UV irradiation (3 × 60 W, Philips type, $\lambda_{max} = 365$ nm). The obtained suspension was washed with 3 × 50 mL H_2O, dried at 80 °C, 24 h. (*Abbreviation: TiO_2/Au_P*).

2.3. Methods and Instrumentation

2.3.1. Diffuse Reflectance Spectroscopy (DRS)

To analyze the optical properties of the composites, diffuse reflectance spectroscopy was used (*JASCO-V650* spectrophotometer with an integration sphere (ILV-724), λ = 250–800 nm). By using the Kubelka-Munk equation/ Tauc plots the indirect band-gap energy values were estimated for the obtained nanomaterials.

2.3.2. X-ray Diffraction (XRD)

In order to investigate the crystal phase composition of the semiconductors and composites, XRD measurements were performed on a *Rigaku* diffractometer ($\lambda_{CuK\alpha}$ = 0.15406 nm, 40 kV, 30 mA, in the 20–40° (2θ°) range) using a graphite monochromator.

2.3.3. Transmission Electron Microscopy (TEM)

To investigate the morphology and the size of the as obtained nanostructures, TEM micrographs were acquired, using a *FEI Technai* G2 20 X-TWIN instrument, operating at 200 kV, using Formvar coated copper grids.

2.4. Photocatalytic Measurements

The photocatalytic activity was assessed by the UV light driven degradation of model pollutants (methyl orange and phenol), analyzing in detail the evolution of the degradation intermediates for phenol. The photocatalytic measurements in the case of phenol were carried out in a double walled photoreactor (100 mL), surrounded by a thermostating jacket (25 °C). The solution was continuously stirred and irradiated by six fluorescent lamps (each lamp with 6 W power, emission maximum at 365 nm, where the distance of the light source from the reactor is ≈5 cm). The phenol concentration changes and the evaluation of intermediates' concentration profile was measured by HPLC system (*Merck-Hitachi L-7100* with low-pressure gradient pump, equipped with a *Merck-Hitachi L-4250* UV-Vis detector and a *Lichrospher Rp* 18 column applying methanol/water mixture as eluent using 210 nm as the detection wavelength). For the comparison of the degradation rate an empirical approximation was used, abbreviated as IEI (intermediates evolution index).[29,30] The catalysts IEI numbers do not depend by the totally degraded phenol quantity (therefore can be compared the all used catalysts, without carrying out the experiment until all the phenol is removed). The IEI number can be calculated by integrating the area below of function F_{int} (the experimental concentration data describing mathematical expression of the given degradation intermediate) until the considered phenol degradation yield is achieved at the phenol concentration value (C_{phenol}) determined universally for all the composites.

$$\mathrm{IEI} = \int_0^{C_{phenol}} F_{int}\, dC \tag{1}$$

In the case of methyl orange we used nearly the same instrumentation. The decrease of methyl orange concentration was measured by JASCO-V650 spectrophotometer (the methyl orange absorption maximum, which can be found at 513 nm, in aqueous solution).

3. RESULTS AND DISCUSSION

3.1. Characterization of the Photocatalysts Optical Properties and Materials' Structure

We have successfully characterized the optical parameters of the composites by using DRS, while their morphology was confirmed by TEM. The characteristic plasmonic bands of gold nanoparticles appeared at the appropriate wavelengths. In the literature these were identified between 520–580 nm.[31–33] The shape and location of the plasmonic band was dependent on the nanoparticles' size and morphology. The plasmonic bands of the as obtained composites appear between 534–568 nm. The TiO_2/Au_S plasmonic band maximum was at 534 nm suggesting 10 nm ± 2 nm sized[34] nanoparticles. The gold nanowires identified showed ≈10 ± 2 nm diameter and > 1 μm length, showing and optical response at 550 nm (Fig. 1).[35] Along the nanowires a smaller fraction of nanospheres were detected similar to those in the case of Au_S. This can be attributed due to very similar reaction parameters, where presumably the wires were built from the small spheres. Due to this morphological change a red shift was noted on the absorbance spectra compared to the plasmonic band maximum of the nanospheres. In the case of Au_T (gold nanotriangle) shaped particles with ≈100–150 nm lateral length were obtained, showing an absorption maximum at 573 nm.[36] The composites containing Au nanoparticles obtained by photoreduction method showed an absorption maximum around 543 nm, suggesting a particle size ≈20 ± 4 nm.[37]

The composites band-gap energy was lower (2.70–2.85 vs. 3.15 eV) than the reference catalysts band-gap, therefore the energy needed for the activation process could be in the visible light region (Fig. 2).

Using X-ray diffraction measurements, we obtained information about the catalysts' crystal phase composition. From the XRD patterns of the bare TiO_2, we identified the characteristic diffraction peaks of anatase and rutile which were the two crystal phases in a well-defined weight ratio (89% anatase, 11% rutile, data not shown).[38] Furthermore, it was observed that the gold nanoparticles do not induce any changes in the TiO_2 crystal structure, and are quasi-unobservable because of the small concentration of the Au nanoparticles and due to the fact that their most intensive diffraction peak of gold was covered by the anatase triple diffraction peaks, which appeared at 38 ($2\theta°$).[27,39]

3.2. The Photocatalytic Activity of the Obtained Nanomaterials

3.2.1. Photodegradation of Phenol

Generally, it's already known that phenol adsorbs poorly on the catalysts' surface, but its intermediates possess increased adsorption affinity towards the surface of titania.[40] For the degradation of phenol, the obtained composites' efficiency values did not surpass the efficiency of the bare photocatalyst. Comparing the composites, the most active photocatalyst was the TiO_2/Au_W (71.01%) and with the lowest activity TiO_2/Au_T (50.50%) was registered (Fig. 3). The order of degradation efficiencies was: TiO_2/Au_W > TiO_2/Au_P > TiO_2/Au_S > TiO_2/Au_T.

For explanation of the lowered degradation yields obtained in the case of Au-based composites it was proposed that the increased efficiency of charge separation promotes the formation of $^{\cdot}OH$ on the surface of the catalysts and these radicals are enhancing the formation of intermediates which are multiply hydroxylated. On the

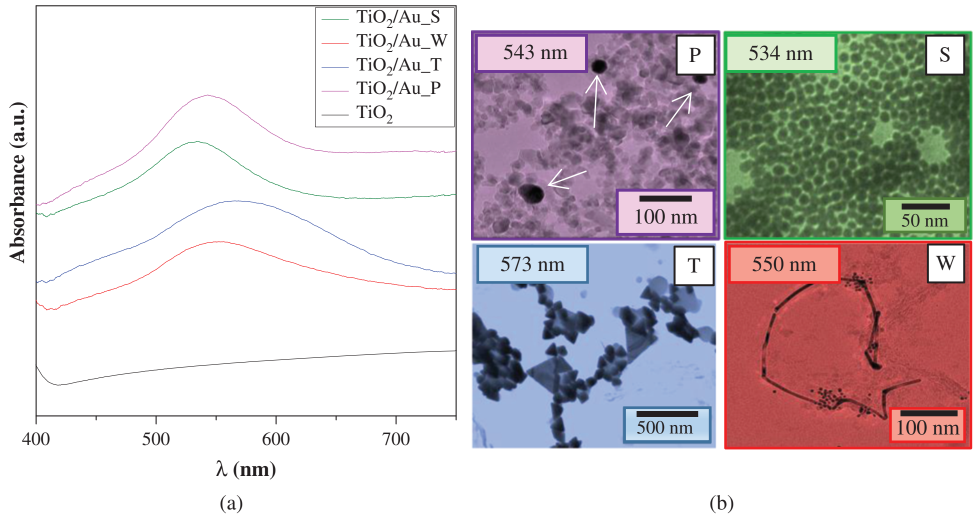

Figure 1. (a) DRS spectra of TiO_2/Au composites; (b) TEM micrographs of the gold nanoparticles (P: photoreduction, S: spheres, T: triangles, W: wires).

other hand, these intermediates can absorb with higher efficiency on the surface of the catalyst, blocking in this way the main reaction site for phenol.

3.2.2. Photodegradation of Methyl Orange

Taking into account the obtained degradation yields for photodegradation of phenol, the two best performing composites were selected in order to check if the activity trend is valid for in this case as well. The unmodified commercial photocatalyst degraded 82.82% of the methyl orange while the composites modified with Au nanoparticles showed similar photocatalytic efficiencies as the base photocatalyst (TiO_2/Au_W (82.68%), TiO_2/Au_P (76.03%), Fig. 4). It has to be mentioned, that the activity order has valid also for this model pollutant/organic dye (the TiO_2/Au_W had higher efficiency as the TiO_2/Au_P).

3.2.3. Intermediates Evolution for Photodegradation of Phenol

The primary intermediate degradation products of phenol are PY, Res and HQ and the second step degradation intermediates are 1,3,5 trihydroxy-benzene and the 1,2,4

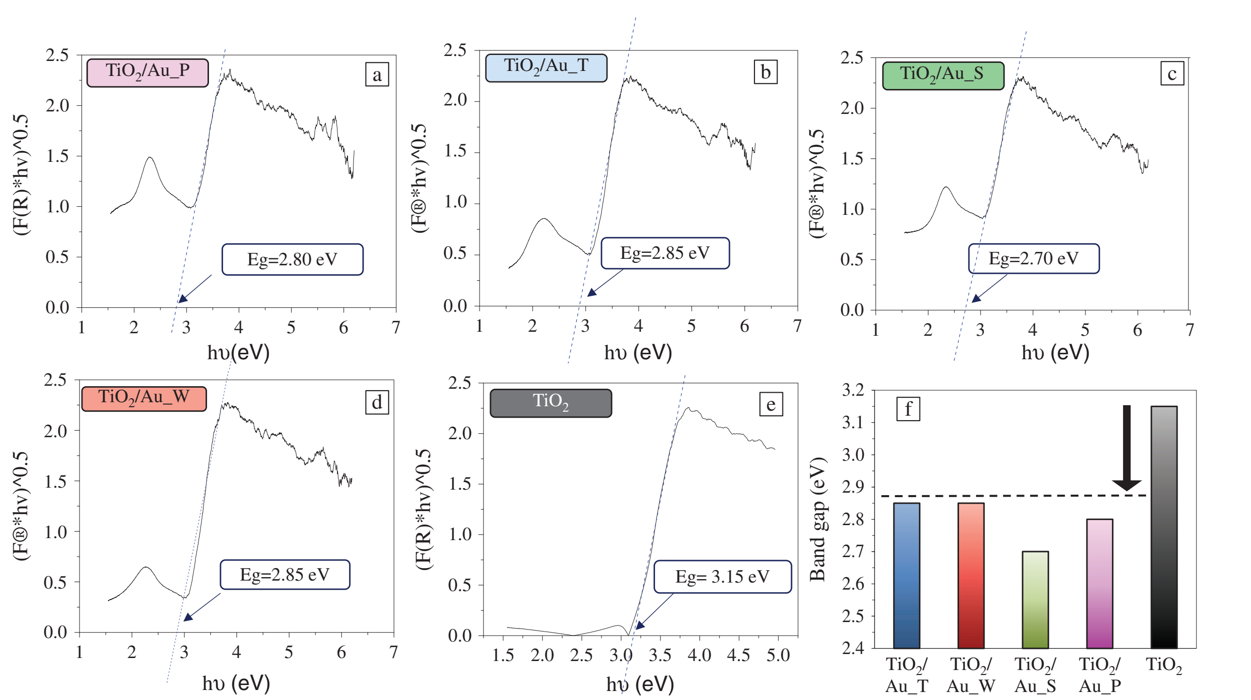

Figure 2. (a–e) Kubelka-Munk transformation/Tauc plots for the calculation of the indirect band-gap value of the bare catalysts and the composites (a) TiO_2/Au_P; (b) TiO_2/Au_T; (c) TiO_2/Au_S; (d) TiO_2/Au_W; (e) TiO_2); (f) comparison of the obtained band-gap values.

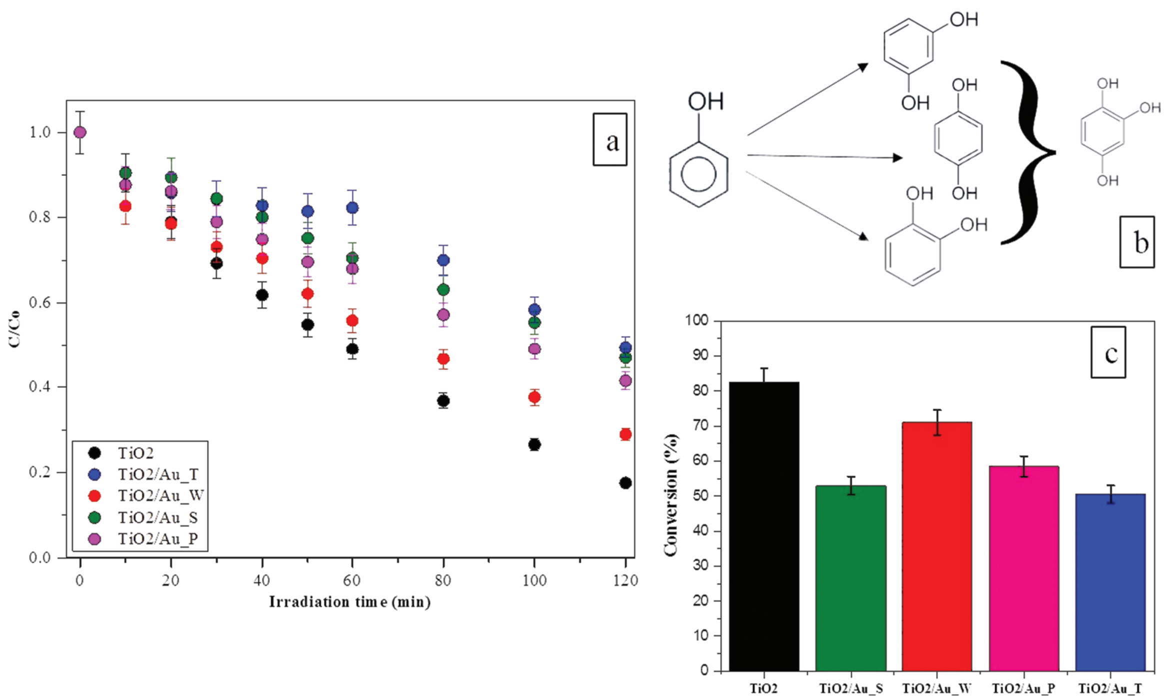

Figure 3. The photodegradation of phenol (a: the degradation curve; b: examined phenol intermediates; c: conversion rates).

trihydroxy-benzene, but the present work focuses only on the formation of 124 THB.

The composites based on spherical and triangle shaped gold nanoparticles were the least active composites, which could be attributed to the intermediates adsorption in the catalysts surface. If the intermediates block the surface of the catalyst, the degradation of the phenol is inhibited as its degradation is carried out by the ·OH radicals, which are most probably not forming, while intermediate molecules were present.

During the photooxidation of phenol the formation of HQ and PY are favored, but from environmental approach, the formation of HQ is preferable as a possible degradation intermediate taking into account the LD_{50} values of the evaluated degradation intermediates. As it can be seen in Figure 5 the formation of PY was the highest in case of TiO_2, while the IEI number of HQ was lower, than in the case of the composite photocatalysts. From these results we can conclude when more HQ was formed, less PY was generated by the photodegradation process.

In the case of TiO_2/Au_W sample PY is the favorable product, and the HQ formation was suppressed. In the case of TiO_2 the same trend was observed. When TiO_2/Au_S and TiO_2/Au_P samples were investigated we observed,

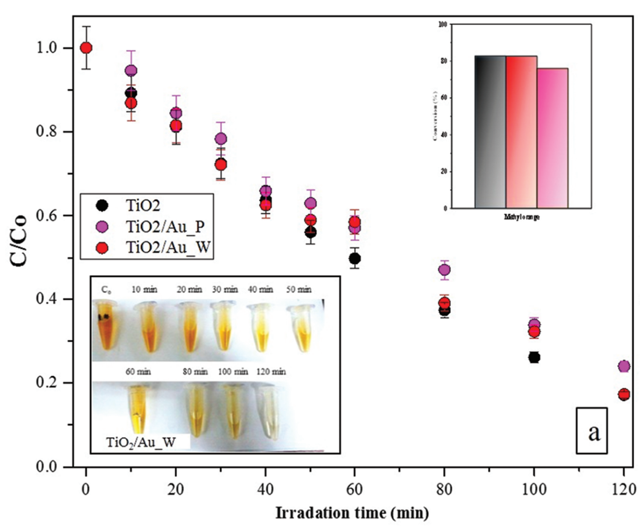

b	r_0, methyl orange (μM/min)	Conversion (%)
TiO_2	1.48	82.82
TiO_2/Au_W	1.47	82.68
TiO_2/Au_P	0.83	76.03

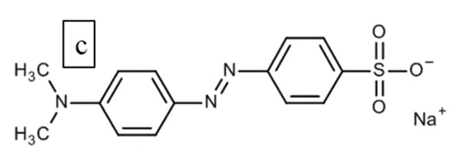

Figure 4. Photocatalytic degradation of methyl orange (a: degradation curves, b: the initial reaction rates/conversion values; c: molecular structure of methyl orange).

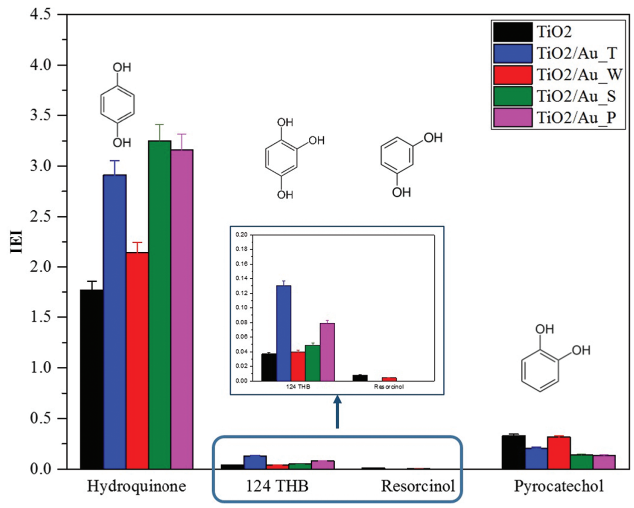

Figure 5. The IEI numbers of the detected intermediates.

that low phenol degradation resulted in the accumulation of HQ and low quantities of PY. A correlation was also observed between 124 THB IEI value and the low HQ evolution values for TiO_2/Au_T samples. The formation of 124 THB showed a high IEI value, when HQ IEI is lower. 124 THB has higher LD_{50} values than the HQ, it can be considered that we produced a more toxic product, but 124 THB easily could transform at other intermediates as well. In case of resorcinol, lower IEI number was calculated when TiO_2/Au_W and bare photocatalysts were used, while for other composites the formation of RES was insignificant/below of the detection limit of the method.

Also, a high yield of phenol degradation was directly correlated with the formation of PY. Because PY is the most toxic primary intermediate of phenol, bare TiO_2 is less desired for shorter degradation processes, even if it showed the highest phenol degradation rate. TiO_2/Au_W composite also showed good conversion values, although their registered PY and Res IEI values were high, which from the environmental point of view are not favorable intermediates.

In the case of noble metal containing composites the evolution of HQ was opposite comparing to the band-gap energies. It can be also observed that the TiO_2/Au_S, which differs from TiO_2/Au_W from ≈10 °C in the synthesis, degraded 52.98% of phenol and it is the most active catalyst in HQ generation, according to the calculated IEI values. TiO_2/Au_P was found to be an appropriate photocatalyst because showed 58.46% degradation form the total amount of phenol. Besides of this it evaluated a big amount of the HQ. The lower HQ values, than the TiO_2/Au_S, probably due from the 124 THB evaluation (probably the HQ transformed to 124 THB).

4. CONCLUSIONS

In the present work we demonstrated the influence of the different shaped gold nanoparticles on the activity of TiO_2. The used crystal morphologies were spheres (using two different reaction pathways), wires and triangles. The composites band-gap energies values were lower than the value of the bare catalysts, having a strong correlation with the degradation efficiency values of phenol. We could also observe that the modification of the commercial TiO_2 with Au nanoparticles can slightly inhibit the efficiency of the photocatalyst toward phenol. Furthermore, it can increase the degradation yields toward other model pollutants or can influence the photodegradation pathway of phenol on benefic routes, forming less harmful degradation intermediates in the case of phenol (forming hydroquinone instead of other intermediates, like 124-THB having have much smaller LD_{50} values).

Acknowledgments: The authors would like to acknowledge the financial support of Swiss Contribution SH 7/2/20. Zsolt Pap and Gábor Kovács wants to acknowledge the financial support of Hungarian Academy of Sciences.

References and Notes

1. A. J. Haider, R. H. Al-Anbari, G. R. Kadhim, and C. T. Salame, *Energy Procedia* 119, 332 (**2017**).
2. G. Žerjav, M. S. Arshad, P. Djinović, J. Zavašnik, and A. Pintar, *Applied Catalysis B: Environmental* 209, 273 (**2017**).
3. P. Cheng, Y. Wang, L. Xu, P. Sun, Z. Su, F. Jin, F. Liu, Y. Sun, and G. Lu, *Mater. Lett.* 175, 52 (**2016**).
4. A. Ayati, A. Ahmadpour, F. F. Bamoharram, B. Tanhaei, M. Manttari, and M. Sillanpaa, *Chemosphere* 107, 163 (**2014**).
5. S. Demirci, T. Dikici, M. Yurddaskal, S. Gultekin, M. Toparli, and E. Celik, *Appl. Surf. Sci.* 390, 591 (**2016**).
6. M. Alam Khan, M. Shaheer Akhtar, S. I. Woo, and O. B. Yang, *Catal. Commun.* 10, 1 (**2008**).
7. Z. Wu, Z. Sheng, Y. Liu, H. Wang, N. Tang, and J. Wang, *J. Hazard. Mater.* 164, 542 (**2009**).
8. T. S. Natarajan, J. Y. Lee, H. C. Bajaj, W.-K. Jo, and R. J. Tayade, *Catal. Today* 282, 13 (**2017**).
9. E. Priyadarshini and N. Pradhan, *Sensors and Actuators B: Chemical* 238, 888 (**2017**).
10. S. Her, D. A. Jaffray, and C. Allen, *Advanced Drug Delivery Reviews* 109, 1 (**2017**).
11. M. Singh, D. C. C. Harris-Birtill, S. R. Markar, G. B. Hanna, and D. S. Elson, *Nanomedicine: Nanotechnology, Biology and Medicine* 11, 2083 (**2015**).
12. M. H. Jazayeri, H. Amani, A. A. Pourfatollah, H. Pazoki-Toroudi, and B. Sedighimoghaddam, *Sensing and Bio-Sensing Research* 9, 17 (**2016**).
13. B. Marco, N. R. Shilpa, and L. S. Keun, *Nanotechnology* 21, 285607 (**2010**).
14. C.-J. Huang, Y.-H. Wang, P.-H. Chiu, M.-C. Shih, and T.-H. Meen, *Mater. Lett.* 60, 1896 (**2006**).
15. D. V. R. Kumar, A. A. Kulkarni, and B. L. V. Prasad, *Colloids and Surfaces A: Physicochemical and Engineering Aspects* 422, 181 (**2013**).
16. Y. Sun and Y. Xia, *Journal of American Chemical Society* 126, 3892 (**2004**).
17. W. Chen, S. Cai, Q.-Q. Ren, W. Wen, and Y.-D. Zhao, *Analyst* 137, 49 (**2012**).
18. L.-N. Ma, D.-J. Liu, and Z.-X. Wang, *Chinese Journal of Analytical Chemistry* 38, 1 (**2010**).
19. P. R. Teixeira, M. S. C. Santos, A. L. G. Silva, S. N. Báo, R. B. Azevedo, M. J. A. Sales, and L. G. Paterno, *Colloids Surf. B. Biointerfaces* 148, 317 (**2016**).

20. Y. Gao, X.-B. Fan, W.-F. Zhang, Q.-S. Zhao, G.-L. Zhang, F.-B. Zhang, and Y. Li, *Mater. Lett.* 130, 1 **(2014)**.
21. M. M. Khan, J. Lee, and M. H. Cho, *Journal of Industrial and Engineering Chemistry* 20, 1584 **(2014)**.
22. R. S. Sonawane and M. K. Dongare, *J. Mol. Catal. A: Chem.* 243, 68 **(2006)**.
23. P. Wongwisate, S. Chavadej, E. Gulari, T. Sreethawong, and P. Rangsunvigit, *Desalination* 272, 154 **(2011)**.
24. J. Li, Suyoulema, W. Wang, and Sarina, *Solid State Sciences* 11, 2037 **(2009)**.
25. E. Grabowska, J. Reszczyńska, and A. Zaleska, *Water Res.* 46, 5453 **(2012)**.
26. Z.-R. Tóth, G. Kovács, K. Hernádi, L. Baia, and Z. Pap, *Sep. Purif. Technol.* 183, 216 **(2017)**.
27. Z. Pap, Z. Tóth, V. Danciu, L. Baia, and G. Kovács, *Materials* 8, 162 **(2015)**.
28. K. Mogyorósi, Á. Kmetykó, N. Czirbus, G. Veréb, P. Sipos, and A. Dombi, *React. Kinet. Catal. Lett.* 98, 215 **(2009)**.
29. L. Baia, A. Vulpoi, T. Radu, T. Karácsonyi, A. Dombi, K. Hernádi, V. Danciu, S. Simon, K. Norén, S. E. Canton, G. Kovács, and Z. Pap, *Applied Catalysis B: Environmental* 148–149, 589 **(2014)**.
30. G. Kovacs, L. Baia, A. Vulpoi, T. Radu, E. Karacsonyi, A. Dombi, K. Hernadi, V. Danciu, S. Simon, and Z. Pap, *Applied Catalysis B-Environmental* 147, 508 **(2014)**.
31. X. Huang and M. A. El-Sayed, *Journal of Advanced Research* 1, 13 **(2010)**.
32. T. Felicia, B. Monica, B. Lucian, and A. Simion, *Nanotechnology* 18, 255702 **(2007)**.
33. Z. Pap, I. J. Hidi, G. Melinte, L. Diamandescu, T. Popescu, L. Baia, V. Danciu, and M. Baia, *Chinese Journal of Catalysis* 34, 734 **(2013)**.
34. Z. Jian, H. Liqing, W. Yongchang, and L. Yimin, *Physica E: Low-Dimensional Systems and Nanostructures* 25, 114 **(2004)**.
35. S. Cai, X. Xiao, X. Ye, W. Li, and C. Zheng, *Mater. Lett.* 166, 51 **(2016)**.
36. A. Patel, A. Kumar, and T. Mohanty, Photoreduction Altered Work Function of Au-TiO_2 Nanoparticles Measured by Scanning Kelvin Probe Microscopy **(2013)**, Vol. 13, p. 8217.
37. M. Verma, A. Kedia, M. B. Newmai, and P. S. Kumar, *RSC Advances* 6, 80342 **(2016)**.
38. B. Ohtani, O. O. Prieto-Mahaney, D. Li, and R. Abe, *Journal of Photochemistry and Photobiology A: Chemistry* 216, 179 **(2010)**.
39. Z. Cai, Z. Xiong, X. Lu, and J. Teng, *Journal of Materials Chemistry A* 2, 545 **(2014)**.
40. Q. Chi, M. J. Ford, A. Halder, N. S. Hush, J. R. Reimers, and J. Ulstrup, *Current Opinion in Electrochemistry* 1, 7 **(2017)**.
41. G. Rózsa, Z. Kozmér, T. Alapi, K. Schrantz, E. Takács, and L. Wojnárovits, *Catal. Today* 284, 187 **(2017)**.

Received: 2 November 2017. Accepted: 15 February 2018.